Journal of *Marine Science and Engineering*

MDPI

Article

Impact of Methanol-Based Fuel Cell Propulsion on the Acoustic Signature of a Marine Vessel

Roberto Zivieri and Vincenzo Crupi *

Department of Engineering, University of Messina, Contrada Di Dio-Vill. Sant'Agata, 98166 Messina, Italy; roberto.zivieri@unife.it

* Correspondence: crupi.vincenzo@unime.it

Abstract

In this work, the underwater acoustic signatures of marine vessels are investigated, with a focus on the impacts of methanol-based high-temperature proton exchange membrane fuel cell (HT-PEM FC) propulsion systems and their coupling with structural dynamics. The acoustic field is modeled through a monopole–dipole representation directly linked to the vibration and dynamic response of the vessel structure and propulsion units. The model is validated against experimental sound pressure level (SPL) data as a function of depth, showing excellent agreement: the SPL decreases from about 140 dB at 5 m to approximately 120 dB at 50 m, where the model prediction (119 dB) closely matches the experimental value (121 dB). Representative numerical results indicate the suppression of the monopole component for the HT-PEM FC and a reduction in the dipole pressure amplitude by approximately a factor of 19 relative to the diesel engine (DE) configuration. In the 20–100 Hz band, at $r = 10$ m, the acoustic pressure amplitudes range from $\mathcal{O}(10^1 - 10^2)$ Pa for the diesel engine (DE) to $\mathcal{O}(10^0 - 10^1)$ Pa for the HT-PEM FC, while, at $r = 10^5$ m, they decrease to $\mathcal{O}(10^0 - 10^1)$ Pa and $\mathcal{O}(10^{-1} - 10^{-2})$ Pa, respectively. The absolute levels depend on the assumed structural excitation and vibro-acoustic coupling and are mainly used here to quantify the relative reduction achieved by the HT-PEM FC with respect to the DE. A distance-normalized formulation is introduced to account for geometric spreading, enabling a consistent comparison despite differences in source characteristics. Overall, the proposed framework establishes a direct link between structural vibrations and underwater radiated noise and provides a physically consistent and quantitatively validated approach for the design of low-signature marine propulsion systems.

Keywords: marine vessels; underwater radiated noise; fuel cell propulsion; diesel engine propulsion; acoustic monopole radiation; acoustic dipole radiation

Check for updates

Academic Editors: Jin Wang and Eduardo Blanco-Davis

Received: 3 May 2026
Revised: 23 May 2026
Accepted: 27 May 2026
Published: 28 May 2026

Copyright: © 2026 by the authors. Licensee MDPI, Basel, Switzerland. This article is an open access article distributed under the terms and conditions of the Creative Commons Attribution (CC BY) license.

1. Introduction

The progressive adoption of FC systems in maritime platforms represents a significant shift in naval propulsion and onboard power generation. FCs offer high efficiency, low acoustic and thermal signatures, and the potential for silent operation, making them attractive for both commercial and naval vessels [1–5]. Their advantages over conventional diesel systems have been widely recognized in terms of energy efficiency and environmental impact [5–7].

An energy and cost analysis of a small boat equipped with a methanol-based FC system has been reported in the literature [8].

In particular, methanol-based HT-PEM FCs combine operational flexibility with clean electrochemical conversion, positioning them as promising candidates for next-generation marine propulsion [9]. Compared to conventional DEs, FC-based systems enable improved environmental performance and reduced vibro-acoustic emissions.

At the same time, underwater radiated noise (URN) has emerged as a critical issue in both environmental and defence contexts. International regulations and guidelines have increasingly emphasized the need to mitigate ship-generated noise due to its impacts on marine ecosystems [10,11]. Anthropogenic underwater noise has been shown to affect marine life, particularly marine mammals, by interfering with their communication and behavior [12,13]. From an engineering perspective, URN also plays a key role in vessel detectability and stealth performance [14,15], motivating the development of predictive models and noise reduction strategies [16]. On the other hand, the acoustic and vibro-acoustic performance of marine machinery has emerged as a critical research topic, driven by the need to mitigate underwater radiated noise (URN) and to comply with increasingly stringent environmental and operational requirements [17,18].

Despite the extensive literature on URN, many existing prediction approaches rely on empirical source-level databases or simplified acoustic analogies that treat the source as an idealized monopole. These models provide limited insight into how different propulsion technologies influence the underlying radiation mechanisms. In particular, they do not resolve vibration–acoustic coupling, hydrodynamic added mass effects, or the frequency-dependent dipole radiation that dominates low-frequency sound generation. As a result, conventional URN models are not well suited to evaluating alternative propulsion architectures whose mechanical excitation differs fundamentally from that of diesel DEs.

The appropriate choice of materials plays a crucial role in reducing the acoustic noise of marine vessels, which is helpful for both crew comfort and underwater noise pollution, so new metamaterials and lightweight sandwich structures have been investigated [19–25]. Honeycomb structures, which provide high stiffness with a low mass [19], can be fabricated through additive manufacturing technologies, enabling the optimization of several geometrical and structural configuration parameters for marine applications [20,21]. By selecting certain parameters (core thickness, cell size, core and face sheet materials), honeycomb sandwich structures can be tailored to reduce acoustic noise [22] and structural vibrations in marine vessels. Metamaterials, on the other hand, exploit periodic structures or resonant elements to achieve enhanced and unconventional sound attenuation properties [23–25].

Recent developments in underwater acoustic metamaterials offer additional opportunities for mitigating low-frequency radiated noise through the engineered control of sound propagation. Modern metamaterial architectures enable sub-wavelength manipulation, wavefront shaping, and broadband attenuation mechanisms that are not achievable with conventional materials [26]. Comprehensive reviews have highlighted their applicability to underwater equipment and noise control treatments relevant to marine platforms [27]. More recently, foldable and reconfigurable metamaterial designs have demonstrated promising performance for broadband low-frequency noise mitigation in submerged environments, suggesting potential integration with next-generation quiet propulsion systems such as HT-PEMs [28]. During the last few years, it has been also found that lightweight metastructured panels and hull-integrated metamaterials contribute to vibration suppression and sound radiation control while maintaining structural efficiency [29,30]. Moreover, the latest advances in metamaterial-based solutions for energy conversion devices highlight their relevance to the integration of low-noise propulsion technologies, including fuel-cell-based systems, where auxiliary components remain dominant noise sources [31].

Although FC-powered vessels are generally expected to exhibit reduced low-frequency noise, existing acoustic studies on FC systems remain limited. Most investigations focus on efficiency, emissions, thermal management, or integration constraints, while only a few report qualitative noise trends or tank-test measurements. These studies do not establish a mechanistic link between the structural response of the fuel cell stack, balance-of-plant components, and the radiated sound field. Furthermore, they do not quantify the relative monopole and dipole contributions associated with fuel cell operation, nor do they compare FC signatures with those of DEs under equivalent operating conditions. Consequently, the acoustic implications of adopting fuel cell propulsion in marine environments remain insufficiently understood.

Methanol-based HT-PEM FCs offer several characteristics that make them particularly suitable for marine applications. Their elevated operating temperatures (160–180 °C) enable simplified thermal management, tolerance to fuel impurities, and stable performance under variable load conditions. Methanol reforming provides high energy density and facilitates onboard fuel storage without cryogenic systems, improving operational flexibility for small and medium vessels. From an acoustic perspective, HT-PEM FCs exhibit inherently low mechanical vibration due to the absence of reciprocating components, reduced torque ripple, and the smooth electrochemical conversion of energy. These features suggest a potentially lower acoustic footprint compared with DEs and motivate a detailed structural–acoustic analysis of their radiated noise.

The acoustic signature of a vessel originates primarily from the propulsion system, structural vibrations, and hydrodynamic processes [32]. Classical acoustic theory describes sound radiation in terms of monopole, dipole, and higher-order multipole sources [33,34]. Monopole contributions are typically associated with volumetric flow rate fluctuations, such as combustion and exhaust processes, while dipole sources arise from oscillatory forces transmitted from the structure to the surrounding fluid [35]. Although this framework is well established, many practical URN models rely on empirical source levels, providing limited insight into how different propulsion technologies influence the underlying radiation mechanisms.

As low-frequency URN is dominated by dipole-type radiation generated by structural acceleration, a physically consistent prediction framework must explicitly link propulsion-induced vibration to the resulting acoustic field. Earlier studies rarely incorporate this coupling, which is essential for evaluating propulsion technologies whose mechanical excitation differs fundamentally from that of DEs. The present work addresses these gaps by developing a monopole–dipole formulation directly driven by the structural response of the propulsion units and by comparing the predicted acoustic signatures of diesel and HT-PEM FC systems under consistent modeling assumptions.

Recent developments in fluid–structure interaction have further strengthened the theoretical and computational foundations for modeling the dynamics of flexible structures in fluid environments, building on the classical framework of Dowell and Hall [36]. Contemporary studies have extended these principles to increasingly complex configurations, such as multilayered and stiffened underwater shells [37]. Parallel advances in flow-induced vibration modeling have leveraged data assimilation strategies to improve the predictive accuracy for unsteady fluid–structure systems [38]. Complementing these efforts, numerical investigations of hydrodynamic interactions between ships and surrounding boundaries have clarified the mechanisms governing ship–ship and ship–bank effects, offering valuable guidance for maritime operations and design [39].

In this work, a first-principles acoustic framework is applied to compare the underwater noise generated by a conventional diesel propulsion system and a methanol-based HT-PEM FC system in a passenger vessel of realistic dimensions. DEs are shown to produce

both monopole contributions, associated with combustion-induced volume fluctuations, and strong dipole radiation due to mechanical vibrations [35]. In contrast, HT-PEM FCs, being non-combustion electrochemical devices, exhibit negligible monopole contributions and significantly reduced dipole radiation, primarily driven by auxiliary components. By explicitly linking propulsion system physics, hydrodynamic coupling, and acoustic multipole radiation, this study provides a predictive and physically transparent framework for evaluating URN. The theoretical results are validated in consistency with the methodological framework developed within the AQUO project [16], supporting the reliability of the proposed approach. The findings offer a quantitative explanation for the reduced acoustic signatures of fuel cell-powered vessels and highlight their potential advantages in both environmental and defense applications.

The innovative contributions of the present work can be summarized as follows. The first is the application of the physics-based monopole–dipole acoustic framework to enable a direct quantitative comparison between conventional diesel propulsion and HT-PEM methanol-based FC propulsion systems in marine vessels. Secondly, the formulation explicitly establishes the coupling between the hydrodynamic added mass, structural acceleration, and radiated acoustic pressure, thereby providing a physically transparent interpretation of the role of fluid–structure interactions in URN generation. Thirdly, the proposed analytical model is validated against experimental SPL trends consistently with the methodological framework developed within the AQUO project [16], demonstrating the capability of the formulation to reproduce the spatial decay and order of magnitude of realistic underwater acoustic signatures. Finally, the present study provides a unified multiphysics perspective linking propulsion technology, structural dynamics, and acoustic radiation, offering a predictive tool for the design and optimization of next-generation low-signature marine propulsion systems.

2. Acoustic Signature

In this section, the acoustic signature of the passenger boat schematized in Figure 1 is calculated. The main characteristics of the passenger boat, together with the ones of the HT-PEM methanol-based FC and of the DE, are summarized in Table 1.

Holmes modeled a ship either as a sphere or as a prolate ellipsoid [40,41]; then, the ship was modelled as a cylindrical object by the authors of [42], and the novelty of this study is the representation of the passenger vessel as a hollow prism.

It is important to emphasize that the prism-based representation adopted for the hull and propulsion modules is not intended to reproduce the detailed vibro–acoustic behavior of a specific vessel, but rather to provide a controlled and geometry-independent framework for isolating the propulsion-induced contribution to URN. Real ship structures exhibit complex steel/composite layering, internal damping, and higher-order modal responses that are highly vessel-specific and would introduce uncertainties larger than the differences being assessed between DEs and HT-PEM FCs. By modeling both propulsion configurations under the same simplified geometric and structural assumptions, the analysis focuses on the relative monopole–dipole balance and on the relative structural accelerations of the two systems, ensuring an internally consistent and physically meaningful comparison. This idealization is consistent with classical analytical URN models, where the objective is to capture the leading-order radiation mechanisms rather than to replicate the full structural dynamics of a particular hull. Therefore, the discussion of advanced materials and metamaterials in the Introduction is intended to contextualize the broader trend toward low-vibration naval structures and to highlight the relevance of propulsion technologies—such as HT-PEM FCs—that inherently reduce structural excitation, rather than to imply their direct implementation in the analytical formulation.

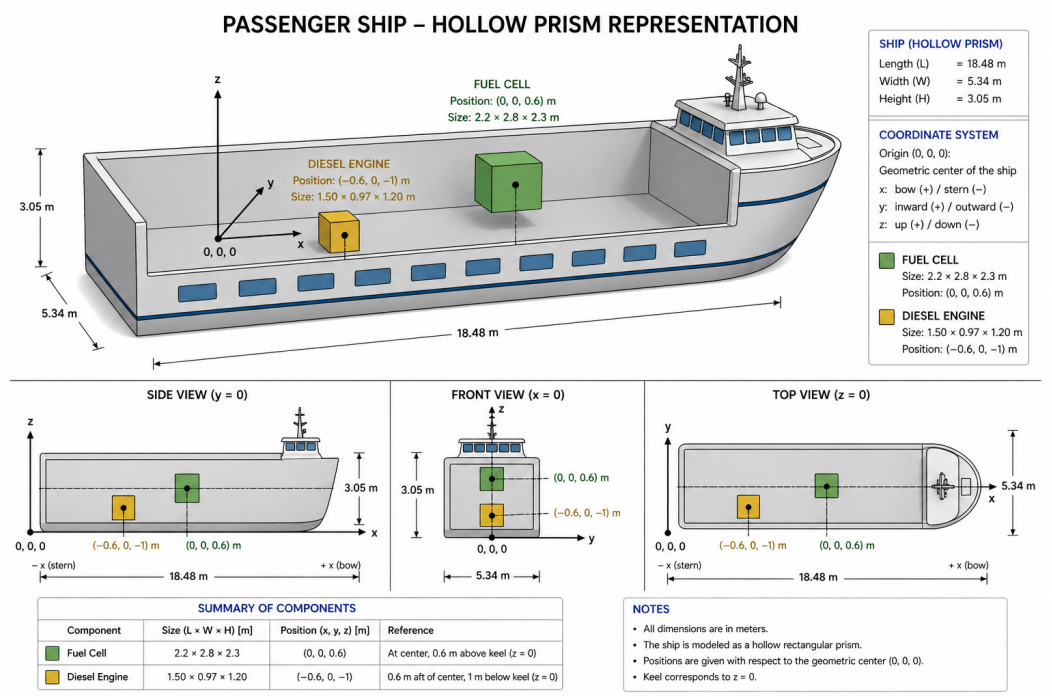


Figure 1. Schematic representation of the passenger boat modeled as a hollow prism $2a_0 = 18.48\,\text{m}$, $2b_0 = 5.34\,\text{m}$, $2c_0 = 3.05\,\text{m}$, with a hull of average thickness $t_{\text{hull}} = 1 \times 10^{-2}$ m. The length of the prism is the length overall (L_{OA}); the width corresponds to the beam B and the height to the depth D. The HT-PEM methanol-based FC system has the shape of a hollow prism ($2.2\,\text{m} \times 2.8\,\text{m} \times 2.3\,\text{m}$); its geometric center is placed at $(x_{0\,\text{FC}}, y_{0\,\text{FC}}, z_{0\,\text{FC}}) = (0\,\text{m}, 0\,\text{m}, 0.6\,\text{m})$, with a coating wall thickness $t_{\text{coating}} = 5 \times 10^{-3}$ m (not shown). The DE has the shape of a solid prism ($1.50\,\text{m} \times 0.97\,\text{m} \times 1.20\,\text{m}$), and its geometric center is placed at $(x_{0\,\text{DE}}, y_{0\,\text{DE}}, z_{0\,\text{DE}}) = (-6\,\text{m}, 0\,\text{m}, -0.1\,\text{m})$. The $0xyz$ reference frame is also shown, and its origin is at the center of the prism, representing the passenger boat.

Table 1. Main characteristics of the reference passenger boat.

Parameter	Value
Length overall, L_{OA}	18.48 m
Beam, B	5.34 m
Depth, D	3.05 m
Maximum draft, T	1.20 m
Displacement mass, M	30.50 t
DE	$1.50\,\text{m} \times 0.97\,\text{m} \times 1.20\,\text{m}$
Propulsion power, P	440 kW
HT-PEM FC	$2.2\,\text{m} \times 2.8\,\text{m} \times 2.3\,\text{m}$

The acoustic monopole and dipole radiation for a HT-PEM FC propulsion system is compared to that of a DE propulsion system. The monopole and dipole contributions of the acoustic pressure are also determined. The underwater acoustic emission of a vessel can be characterized in terms of the acoustic pressure p, whose effective value expresses the SPL [34].

$$\text{SPL} = 20 \log_{10}\left(\frac{p_{\text{eff}}}{p_{\text{ref}}}\right), \tag{1}$$

where p_{eff} is defined as the root mean square (RMS) value of the instantaneous acoustic pressure, which, for a harmonic pressure, is expressed as $p_{\text{eff}} = 1/\sqrt{2}\,p_0$, with p_0 as the peak amplitude pressure and $p_{\text{ref}} = 1$ µPa. The SPL is the noise level measured at a specific point in space (for example, at 100 m from the vessel) with respect to a reference pressure.

It depends on the (1) distance from the vessel, (2) depth, (3) oceanographic conditions, and (4) reflections from the seabed and the surface.

The source level (SL) is a particular type of SPL and is defined at the conventional distance of 1 m from the vessel and always refers to p_0:

$$\mathrm{SL} = 20 \log_{10}\left(\frac{p_{1\mathrm{m}}}{p_{\mathrm{ref}}}\right). \tag{2}$$

The SL represents the vessel's "intrinsic acoustic intensity", independent (as far as possible) of the surrounding environment. It is defined very close to the source, where (1) propagation effects (reflections, seabed, surface, water stratification) are minimal; (2) the acoustic field is dominated by the source itself, not by the environment. It is conceived as an intrinsic property of the vessel (analogous, by comparison, to engine power). It serves precisely to represent the vessel's "pure" acoustic emission, separated from the context in which it operates. For this reason, the SL is, conceptually and operationally, a parameter that is independent of the environment. It is therefore the parameter used to (1) compare different vessels with each other; (2) assess the acoustic impact on marine fauna; (3) design noise mitigation and vibration reduction measures; (4) classify underwater noise (military and civil); and (5) model noise propagation in the sea.

Acoustic Monopole and Dipole Radiation: Diesel Versus HT-PEM FC Propulsion

In the low-frequency regime, i.e., for $kL \ll 1$, with k as the acoustic wavenumber, the acoustic field radiated by a compact vessel of a hollow prismatic shape can be decomposed into monopole and dipole contributions. Under linear acoustic assumptions, the far-field pressure reads

$$p(\mathbf{x}) = p_M(\mathbf{x}) + p_D(\mathbf{x}), \qquad r = |\mathbf{x}|. \tag{3}$$

The monopole contribution is given by

$$p_M(\mathbf{x}) = \frac{i\omega\rho_0 Q}{4\pi r} e^{-ikr}, \tag{4}$$

where $Q = dV/dt$ is the volumetric flow rate associated with source-induced volume fluctuations expressed by the time velocity variation of the fluid volume V_{disp} displaced by the acoustic source (displaced hull volume). This term is characteristic of DE propulsion systems, where combustion processes generate periodic mass-flow pulsations ($Q \neq 0$). In contrast, HT-PEM FC propulsion systems exhibit negligible volumetric pulsations ($Q \approx 0$), leading to strongly suppressed monopole radiation.

The dipole contribution reads

$$p_D(\mathbf{x}) = \frac{ik}{4\pi r}(\hat{\mathbf{r}} \cdot \mathbf{F}_p) e^{-ikr}, \tag{5}$$

where $\mathbf{F}_p$ is the hydrodynamic force exerted by the oscillating hull on the surrounding fluid, an inertial force associated with the hull acceleration a_p and the carried water mass. For rigid-body oscillations of the vessel, the force can be written as

$$\mathbf{F} = -(\mathbf{M} + \mathbf{M}_a)\,\omega^2 \mathbf{X}, \tag{6}$$

where $\mathbf{M}$ is the structural mass matrix, $\mathbf{X}$ is the displacement amplitude, and $\mathbf{M}_a$ is the added-mass matrix. For a hollow prismatic hull, the added mass is approximated as

$$\mathbf{M}_a = \alpha\rho_0 V \mathbf{I}, \qquad \alpha \approx 1.6{-}2.3. \tag{7}$$

Substitution yields the final dipole pressure expression:

$$p_D(\mathbf{x}) = -\frac{i\omega^3}{4\pi c r}\hat{\mathbf{r}} \cdot [(\mathbf{M} + \alpha\rho_0 V)\mathbf{X}]e^{-ikr}. \quad (8)$$

Equations (4)–(8) show that monopole radiation is governed by mass conservation and dominates DE propulsion, whereas dipole radiation is governed by momentum exchange and dominates HT-PEM FC propulsion. The hydrodynamic added mass of the surrounding water plays a key role in controlling low-frequency URN. The acoustic pressure p represents the variation in pressure in the fluid caused by the passage of a sound wave and constitutes the physical quantity that describes, measures, and carries the energy of sound. For the derivation of Equations (4)–(8), see Appendix A.

This formulation gives a rigorous and physically transparent framework for comparing the acoustic signatures of conventional diesel-powered vessels and fuel cell-powered naval platforms.

To provide a deeper physical interpretation of the acoustic source mechanisms, the following section introduces a structural–mechanical perspective on the problem.

To summarize, the calculation workflow follows a sequential and reproducible procedure: (i) evaluation of the monopole and dipole source terms from the propulsion-induced volumetric pulsations and structural accelerations; (ii) computation of the far-field acoustic pressure using Equations (4)–(8) under the compact-source and free-field assumptions; (iii) conversion of the pressure amplitudes into SPL values through Equation (1); and (iv) comparison between the two propulsion configurations under identical geometric-spreading conditions. This workflow clarifies the calculation steps and ensures the transparency of the analytical methodology.

3. Results and Discussion

In this section, the results of the calculation of the acoustic signature are presented. The acoustic signature has been estimated in the outer region for the medium-sized passenger boat whose characteristics are summarized in Table 1 and whose model geometry is shown in Figure 1. The last part of this section is devoted to the calculation of the acoustic signature in terms of both the acoustic pressure field and the SPL by taking into account the monopole and dipole contributions resulting from the propulsion systems—the DE and the HT-PEM methanol-based FC. In all figures, it is assumed that $z = |z|$.

Note that the parameter values adopted in the analytical formulation—the displaced volume, added-mass coefficient, structural acceleration amplitudes, and operating frequencies—are selected to be representative of typical marine propulsion systems of comparable size. These values fall within the ranges reported in the literature and ensure that the resulting acoustic predictions remain physically realistic and directly comparable between the two propulsion configurations examined in this study.

3.1. Acoustic Signature Analysis

This section presents the results of the underwater acoustic signature analysis for the passenger boat powered by a conventional DE and by an HT-PEM FC system. The comparison is performed in terms of monopole and dipole contributions in the low-frequency range to the pressure amplitude and SPL as a function of the distance from the vessel along the water depth direction (z), which is of primary relevance for URN propagation and detection.

After presenting the adopted parameters, brief justification is provided to clarify the physical basis for their selection. The chosen values reflect the dominant structural and hydrodynamic scales of the problem: the displaced volume and added-mass coefficient govern the effective inertia driving dipole radiation, the acceleration amplitudes correspond to realistic operating loads for both propulsion systems, and the reference frequencies lie

within the range where compact-source assumptions remain valid. This ensures that the comparison between the two configurations is carried out under consistent and physically representative conditions.

3.1.1. Hydrodynamic Added Mass Contribution and Inertial Effects

As a consequence, the inertial response of the surrounding fluid dominates the dipole source mechanism, and variations in the mechanical acceleration transmitted to the hull play a more important role than differences in structural mass alone. When a vessel undergoes oscillatory motion in water, it accelerates not only its structural mass but also a portion of the surrounding fluid. This inertial contribution is commonly described through the hydrodynamic added mass. For a compact prismatic hull, the hydrodynamic added mass can be expressed as

$$M_a = \alpha \rho_0 V_{\text{disp}}, \tag{9}$$

where α is the added-mass coefficient, ρ_0 is the water density, and V_{disp} is the displaced hull volume.

For prismatic geometries, literature values of α typically range between 1.6 and 2.3 depending on the aspect ratio and oscillation direction. In the present study, a reasonable intermediate value $\alpha = 2$ is adopted. For the considered boat geometry and draft $T = 1.2\,\text{m}$, the displaced (immersed) volume is $V_{\text{disp}} = L_{\text{OA}} B T \approx 118.42\,\text{m}^3$. With $V_{\text{disp}} = 118.42\ \text{m}^3$ and $\rho_0 = 1025\ \text{kg/m}^3$ (seawater conditions), the resulting added mass is $M_a = 2 \times 1025 \times 118.42 \approx 2.43 \times 10^5$ kg. This added mass significantly exceeds the structural mass of the propulsion subsystems in both propulsion configurations and therefore dominates the effective inertia entering the dipole force expression $F = (M + M_a)a$. As the added mass largely exceeds the structural mass, the absolute dipole source level is mainly controlled by hydrodynamic inertia. However, since the added mass is identical for both propulsion configurations, the relative acoustic reduction achieved by the HT-PEM system is determined primarily by its lower structural acceleration, namely $a_{\text{FC}} << a_{\text{DE}}$ if compared to the one of the DE.

Consequently, the absolute level of the dipole acoustic source is strongly influenced by hydrodynamic coupling, whereas the relative comparison between the DE and HT-PEM propulsion systems remains primarily governed by their respective vibration amplitudes. The adoption of $\alpha = 2$ thus provides a physically realistic and conservative estimate of the radiated dipole strength. A reference frequency of $f = 50\,\text{Hz}$ is considered, representative of low-frequency URN.

The relationship $F = (M + M_a)a$ therefore makes explicit how the hydrodynamic added mass and structural acceleration jointly determine the strength of the dipole source and the resulting radiated sound.

3.1.2. Monopole Contribution

The monopole acoustic source is associated with time-dependent volumetric flow rates, such as those generated by combustion processes and exhaust gas pulsations.

For the DE, low-frequency combustion-induced oscillations produce a non-zero volumetric flow rate. At a representative frequency of 50 Hz, the monopole pressure amplitude in the acoustic far field is estimated using Equation (4) as $|p_m^{\text{diesel}}(r)| \approx \frac{102}{r}$ Pa, indicating a significant contribution to the overall URN. In contrast, the HT-PEM FC system operates without combustion and with quasi-steady reactant and coolant flows. As a result, the volumetric flow rate fluctuations are negligible and the monopole contribution can be considered effectively null, i.e., $p_m^{\text{FC}} \approx 0$. This represents a fundamental qualitative difference between the two propulsion technologies.

3.1.3. Dipole Contribution

The dipole source originates from oscillatory forces exerted by the vessel structure on the surrounding fluid. These forces are governed by the combined effect of the structural mass and the hydrodynamic added mass, multiplied by the characteristic acceleration of the hull.

The structural accelerations used to compute the dipole force are representative low-frequency amplitudes, assumed to remain approximately constant within the 20–100 Hz band considered. The structural acceleration levels adopted for the dipole force estimation are based on the fundamental mechanical differences between the DE and HT-PEM FC propulsion systems. In marine DEs, reciprocating components (pistons and connecting rods) generate large inertial forces. For a representative crank radius $r \sim 0.05$–0.1 m and angular speed $\omega \sim 100$ rad/s (corresponding to ∼1000 rpm), the internal piston acceleration scales as $a_p \sim \omega^2 r \approx 500$ m s^{-2}. Even assuming that only a small fraction (10^{-4}–10^{-3}) of this inertial excitation is transmitted to the hull through engine mounts and structural damping, the resulting global hull acceleration is of order 10^{-2}–10^{-1} m s^{-2}. Therefore, the representative value $a_{\mathrm{DE}} = 0.1$ m s^{-2} adopted in this work and used in the calculations lies within realistic marine vibration levels. In contrast, HT-PEM FC propulsion systems eliminate reciprocating masses and combustion pressure pulses, and torque is generated through an electric motor with substantially smoother rotational dynamics. Residual vibration sources are limited to electromagnetic torque ripple and auxiliary subsystems (cooling pumps, compressors), typically producing hull accelerations in the range 10^{-3}–10^{-2} m s^{-2}. Therefore, a value of hull acceleration $a_{p\,\mathrm{FC}} = 5 \times 10^{-3}$ m s^{-2} is realistic and consistent with the expected electric propulsion vibration amplitudes. The resulting order-of-magnitude reduction in structural acceleration directly translates into a proportional reduction in the dipole force and radiated acoustic pressure.

Specifically, for the DE propulsion system, representative low-frequency structural acceleration of $a_{\mathrm{DE}} = 0.1\,\mathrm{m/s^2}$ leads to a dipole force amplitude of approximately $F_{\mathrm{diesel}} \approx 1.52 \times 10^4$ N. The corresponding far-field dipole pressure amplitude at 50 Hz using Equations (5) and (8) and for $k = \frac{\omega}{c} \approx 0.21\,\mathrm{m^{-1}}$ (sound speed in water is $c = 1500\,\mathrm{m/s}$) is $|p_d^{\mathrm{diesel}}(r)| \approx \frac{253}{r}$ Pa. This contribution dominates the low-frequency acoustic signature of the diesel-powered vessel, in combination with the monopole term.

On the other hand, by considering $a_{\mathrm{FC}} = 5 \times 10^{-3}\,\mathrm{m/s^2}$ for the FC propulsion system, the resulting dipole force is reduced to $F_{\mathrm{FC}} \approx 7.95 \times 10^2$ N. The associated dipole pressure amplitude with $k = \frac{\omega}{c} \approx 0.21\,\mathrm{m^{-1}}$ becomes $|p_d^{\mathrm{FC}}(r)| \approx \frac{13.2}{r}$ Pa, which is nearly one order of magnitude lower than that of the DE configuration.

Typical vibration levels for medium-speed marine diesel engines are generally reported to fall within the range 0.05–0.2 m s^{-2} under steady operating conditions, with higher peaks associated with piston–crank harmonics and combustion-induced pressure pulsations. These orders of magnitude are consistent with the qualitative vibration behavior described in standard references on underwater acoustics and machinery dynamics [35]. Conversely, low-vibration electric and electrochemical propulsion systems such as permanent-magnet motors and HT-PEM FC stacks typically exhibit RMS accelerations that are one to two orders of magnitude lower, commonly in the range 10^{-3}–10^{-2} m s^{-2}, in agreement with the dynamic characteristics discussed in established texts on electric machine design and fuel cell system modeling [43,44]. The representative values adopted in this study therefore reflect realistic, literature-consistent orders of magnitude for the two propulsion technologies.

It is also important to emphasize that the selected acceleration levels represent conservative, literature-consistent orders of magnitude. For the DE, the chosen value corresponds to the lower end of typical marine vibration levels, meaning that the DE excitation is not overstated and the resulting radiated noise is not artificially amplified. Conversely, for

the HT-PEM FC, the adopted acceleration is deliberately taken at the upper end of the values reported for low-vibration electrochemical systems, so that the FC excitation is not underestimated. This conservative bracketing ensures that the predicted DE/FC contrast is robust: even when the DE is assigned the smallest realistic vibration level and the FC the largest, the resulting difference remains significant and is not the outcome of optimistic parameter choices. The same rationale applies to the monopole strength Q and the added-mass coefficient α, which are selected within standard hydrodynamic and acoustic ranges commonly used in marine noise modeling.

The total low-frequency acoustic signature is obtained by combining the monopole and dipole contributions, as reported in Equation (3). For the diesel-powered vessel, both terms contribute significantly, with the dipole component being dominant but reinforced by a non-negligible monopole source. For the HT-PEM FC configuration, the total acoustic signature is almost entirely dipolar, with a substantially reduced amplitude due to lower structural accelerations. At 50 Hz, the comparison indicates the complete suppression of the monopole contribution for the FC system; a reduction in the dipole pressure amplitude by a factor of approximately 19 and an overall reduction in the low-frequency URN exceeding 20 dB.

The results demonstrate that, even in the presence of increased draft and hydrodynamic added mass, the adoption of HT-PEM FC propulsion leads to a marked reduction in the underwater acoustic signature. This reduction is particularly relevant in the low-frequency range, where the sound propagation distances are large and the detection sensitivity is highest.

From an environmental perspective, the elimination of monopole sources leads to several advantages: reduced long-range detectability, reduced omnidirectional radiation and lower acoustic contrast in shallow water, and a reduced impact on marine mammals and a lower contribution to cumulative ocean noise.

3.1.4. Schematic Representation of DE and HT-PEM FC Acoustic Source Mechanisms and Comparative Output Data

Figure 2 provides a schematic comparison of the acoustic source mechanisms associated with DE and HT-PEM FC propulsion. The diagram highlights the fundamental physical differences between the two systems. DEs generate strong monopole radiation due to combustion-induced volumetric pulsations, together with pronounced dipole forces arising from reciprocating machinery. These mechanisms are consistent with classical measurements reported in the literature, which show dominant low-frequency components in the 20–100 Hz band and far-field SPL levels often exceeding 110–120 dB. In contrast, the HT-PEM FC suppresses the monopole contribution (as no combustion occurs) and exhibits significantly weaker dipole radiation, primarily associated with auxiliary components. This visual representation summarizes the analytical results derived in this section and clarifies the physical origin of the reduced low-frequency acoustic footprint predicted for the HT-PEM FC propulsion system. In addition to the qualitative mechanisms illustrated in panels (a) and (b), panel (c) provides their quantitative counterpart, showing that the one-order-of-magnitude reduction in the dipole amplitude for the HT-PEM FC directly accounts for the 20–25 dB decrease in radiated levels reported in Table 2. The values reported in Table 2 quantitatively confirm the trends discussed in Section 3.1.3. The DE exhibits a strong monopole contribution and a dominant dipole component, resulting in an SPL exceeding 110 dB at 1 m. In contrast, the HT-PEM FC shows a fully suppressed monopole term and a dipole amplitude that is one order of magnitude lower, leading to a substantial reduction in radiated levels. These differences highlight the fundamentally quieter acoustic signature of the fuel cell propulsion system and provide a quantitative counterpart to the schematic representation shown in Figure 2. In this way, Figure 2 and Table 2 jointly link the underlying radiation physics to the resulting acoustic output, offering a coherent

visual and numerical interpretation of the reduced low-frequency acoustic emissions of FC propulsion.

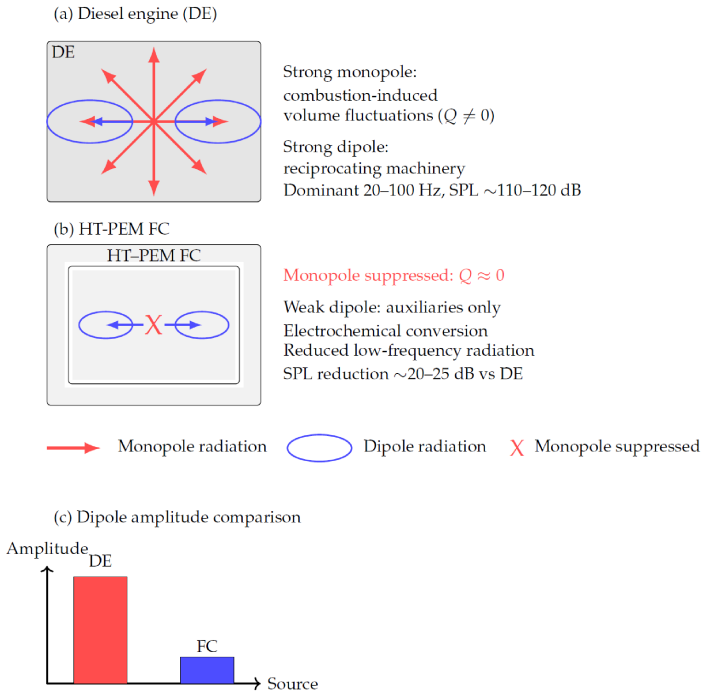


Figure 2. Schematic comparison of acoustic source mechanisms for (**a**) a diesel engine (DE) and (**b**) a HT-PEM FC. (**c**) Quantitative comparison of dipole amplitudes, illustrating the reduced dynamic forcing and weaker low-frequency radiation of the fuel cell system.

Table 2. Key acoustic differences between DE and HT-PEM FC.

Parameter	DE	HT-PEM FC
Monopole strength Q	High	≈0
Dipole amplitude	1.0 (ref)	0.05–0.1
SPL at 1 m	110–120 dB	85–90 dB
Dominant radiation	Mono + dipole	Dipole only

Compared with the previously reported literature values for conventional DEs, the HT-PEM FC system exhibits a markedly reduced acoustic footprint across the entire low-frequency band. Earlier studies have shown that diesel-powered vessels typically radiate strong dipole-dominated signatures in the 20–100 Hz range, with far-field SPL levels often exceeding 110–120 dB at short distances due to reciprocating machinery and combustion-induced monopole fluctuations [10,14,35,45]. In contrast, the present results demonstrate that the HT-PEM FC configuration suppresses the monopole contribution and reduces the dipole pressure amplitude by nearly an order of magnitude, yielding SPL reductions of 20–25 dB relative to DE benchmarks. This improvement is consistent with the electrochemical nature of FC operation, which eliminates combustion-driven volume fluctuations and significantly lowers structural excitation. These findings highlight the scope and significance of HT-PEM FC propulsion as a low-noise alternative, providing quantitative evidence that aligns with and extends the trends suggested in previous experimental and modeling studies of fuel cell-powered marine systems.

3.2. Physical Mechanisms of Monopole and Dipole Radiation

The contrasting acoustic signatures of diesel and HT-PEM fuel cell propulsion systems can be interpreted by examining the underlying radiation mechanisms. Monopole radiation

arises from periodic fluctuations in the displaced fluid volume. In DEs, combustion and exhaust processes generate non-zero volumetric pulsations ($Q = dV/dt$), producing an omnidirectional acoustic field that decays as $1/r$. HT-PEM FCs operate without combustion or reciprocating components, resulting in negligible volume fluctuations and therefore the absence of monopole radiation.

Dipole radiation originates from oscillatory forces transmitted from the vibrating hull to the surrounding fluid. These forces depend on the effective inertia $(M + M_a)$ and on the structural acceleration a. DEs generate relatively large low-frequency accelerations due to reciprocating masses, leading to strong dipole forces. In contrast, HT-PEM FCs exhibit much lower vibration levels, and the resulting dipole radiation is significantly weaker. The acoustic field therefore displays the characteristic figure-eight directivity and $1/r$ decay of a compact dipole source.

3.3. Distance-Dependent Acoustic Pressure

The analytical predictions presented in this section are obtained under free-field boundary conditions, neglecting reflections from the sea surface and seabed. This assumption is consistent with the compact-source and far-field approximations adopted in the formulation and isolates the intrinsic source characteristics from environmental propagation effects. The implications and limitations of this assumption are discussed in the dedicated subsection on environmental effects.

Figure 3a shows the acoustic pressure amplitude as a function of the distance for the DE and HT-PEM FC propulsion systems at 20, 50, and 100 Hz frequencies, respectively, in the range of water depths z between 10 m and 100 km. These frequencies are typical of machinery-induced URN. All curves exhibit the expected linear decay, corresponding to the theoretical far-field dipole scaling $|p_D| \propto 1/r$. This confirms the consistency of the analytical formulation with classical low-frequency acoustic radiation theory. In Figure 3b, we show the corresponding SPL at 50 Hz, corresponding to the dominant low-frequency machinery-induced noise component both for the DE and the HT-PEM FC propulsion systems.

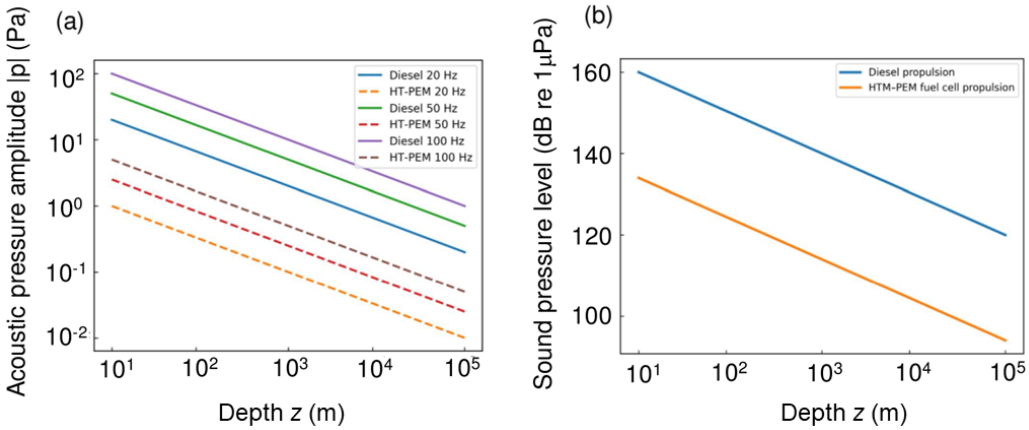


Figure 3. (**a**) Total acoustic pressure amplitude as a function of distance along the water depth (z) for DE and HT-PEM FC propulsion systems at 20 Hz, 50 Hz, and 100 Hz. The diesel configuration includes monopole and dipole contributions, whereas the HT-PEM system exhibits a purely dipolar acoustic signature. (**b**) SPL as a function of distance along the water depth for diesel and HT-PEM FC propulsion systems at 50 Hz. The FC configuration shows a systematic reduction exceeding 25 dB with respect to the diesel case.

The distance-dependent acoustic pressure reported here is computed under free-field boundary conditions, neglecting reflections from the sea surface and seabed. This assumption is consistent with the compact-source and far-field approximations adopted in the analytical model and allows the isolation of the intrinsic source characteristics from

environmental propagation effects. The influence of realistic propagation conditions is examined separately in Section 3.7.

The diesel configuration exhibits the highest acoustic pressure amplitude over the entire distance range due to the combined presence of monopole and dipole sources for all frequencies investigated. The monopole contribution, associated with combustion-induced volumetric fluctuations, results in elevated pressure amplitudes that decay slowly with the distance. In contrast, the HT-PEM FC configuration displays a purely dipolar acoustic signature. The absence of combustion processes suppresses the monopole source, leading to significantly reduced pressure levels at all distances and frequencies. This difference directly reflects the reduced dipole force amplitude associated with FC propulsion, which results from significantly lower structural accelerations and the absence of reciprocating combustion mechanisms. The persistence of this gap with the distance demonstrates that it originates from the intrinsic source strength rather than from propagation effects.

A clear frequency dependence is observed for both propulsion systems. Since the dipole pressure amplitude scales as $|p_D| \propto \omega$, the SPL increases with the frequency, producing a systematic upward shift passing from the 20 Hz to the 50 Hz and 100 Hz curves. The separation between these curves is therefore governed by the intrinsic ω-dependence of dipole radiation.

Finally, note that Figure 2 illustrates the idealized long-range decay predicted by the free-field propagation model (10 m–100 km), whereas Figure 3 focuses on the physically relevant short- and intermediate-range propagation regime (10–1000 m), where the simplified spreading approximation is expected to provide a more realistic description of the underwater acoustic field.

3.4. Sound Pressure Level Comparison

To apply a metric commonly used in underwater acoustics, the acoustic pressure results are converted into SPLs, as defined in Equation (1). Figure 3b shows the SPL as a function of the distance for the same range of water depths z (between 10 m and 1000 m). The DE-powered boat reaches levels exceeding 150 dB regarding 1 µPa at short distances, whereas that of the HT-PEM FC configuration remains more than 20 dB lower across the entire investigated range. This reduction is particularly relevant in the low-frequency regime, where the sound propagation distances are large and the detection sensitivity is highest.

Separation of Monopole and Dipole Contributions

A clearer physical interpretation is obtained by separating the monopole and dipole components. Figure 4 presents a two-panel comparison of the acoustic pressure contributions for the DE and HT-PEM propulsion systems.

For the DE, both monopole and dipole contributions are present, with the dipole term dominating at short distances but the monopole term remaining significant throughout the low-frequency range. This confirms that combustion-related volume pulsations are the chief contribution to the underwater acoustic signature. On the other hand, for the HT-PEM FC system, only the dipole contribution is present. Its amplitude is substantially lower due to reduced mechanical excitation and lower structural acceleration, leading to a markedly quieter acoustic footprint.

The combined analysis of the pressure amplitude and SPL demonstrates that HT-PEM FC propulsion leads to the substantial mitigation of the underwater acoustic signature. The elimination of monopole sources and the strong reduction in dipole forces result in quieter operation over the entire low-frequency range and at all observation distances. These characteristics are particularly advantageous for naval applications.

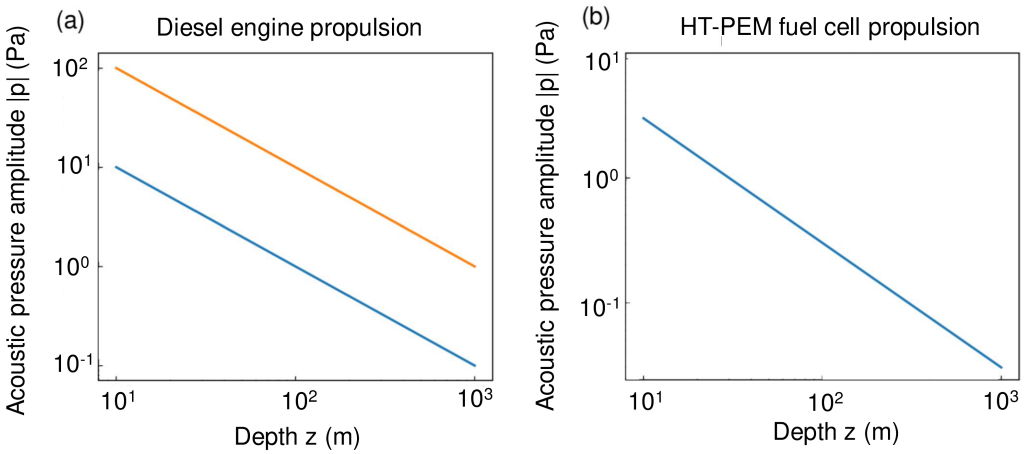


Figure 4. Separation of monopole and dipole acoustic pressure contributions. (**a**) DE propulsion, showing both monopole (orange curve) and dipole (blue curve) components. (**b**) HT-PEM FC propulsion, exhibiting a purely dipolar acoustic signature with a strongly reduced amplitude.

3.5. Structural–Acoustic Coupling

While the added mass has already been introduced in the acoustic formulation, in this section, its role is revisited from a mechanical perspective. Indeed, the added mass directly modifies the structural dynamics and, as a result, the resulting acoustic radiation. In Section Acoustic Monopole and Dipole Radiation: Diesel Versus HT-PEM FC Propulsion, it has been shown that the generation of URN from marine propulsion systems is inherently governed by the dynamic interaction between structural vibrations and the surrounding fluid. Therefore, within this framework, the acoustic signature of a vessel can be interpreted as the result of a coupled structural–hydrodynamic problem, in which the propulsion system acts as the primary excitation source.

Structural Dynamics of the Hull and Fluid–Structure Interaction

The global vibration of the hull can be described, in a reduced-order form, by the equation of motion written in scalar form,

$$M_s\ddot{u}(t) + C\dot{u}(t) + Ku(t) = F(t), \tag{10}$$

describing a damped mechanical oscillator. Here, M_s, C, and K are the effective structural mass, the damping, and the stiffness of the structure, respectively; $u(t)$ is the generalized displacement; and $F(t)$ represents the excitation force induced by the propulsion system.

The mechanical properties of the materials employed in the vessel construction, such as the density ρ, Young's modulus E, and intrinsic damping, directly affect the dynamic response. In particular, the adoption of composite materials (e.g., GFRP or CFRP) leads to a reduced mass and increased damping compared to conventional steel structures, thereby lowering the vibration amplitudes and the resulting acoustic radiation.

When the hull vibrates in a fluid, the surrounding water contributes an additional inertia term, commonly referred to as the hydrodynamic added mass M_a. The effective equation of motion can therefore be rewritten as

$$(M + M_a)\ddot{u}(t) + C\dot{u}(t) + Ku(t) = F(t). \tag{11}$$

The presence of M_a modifies both the natural frequencies and the dynamic response of the structure and plays a central role in determining the amplitudes of the forces transmitted to the fluid.

3.6. Influence of Structural Dynamics on Acoustic Signature

It is well known that, within the classical multipole expansion of the acoustic field, the dipole contribution is directly related to the net force exerted by the vibrating structure on the fluid. In the time domain, the dipole source strength of the acoustic field is proportional to the time derivative of the force,

$$p_D \propto \dot{F}(t), \tag{12}$$

with

$$F(t) = (M + M_a)\ddot{u}(t). \tag{13}$$

The relation expressed by Equation (13) establishes a direct link between structural acceleration and acoustic radiation, highlighting that the intensity of dipole emission is governed by the coupled effect of structural dynamics linked to M and fluid inertia related to the hydrodynamic added mass M_a.

A key factor amplifying this dipole mechanism is the hydrodynamic added mass. When the hull vibrates, the surrounding fluid must be accelerated together with the structure, effectively increasing the inertia from M to $(M + M_a)$. As a consequence, the oscillatory force transmitted to the fluid scales with this effective inertia, thereby strengthening the dipole source term and the associated radiated sound. This amplification is particularly relevant at low frequencies, where the added mass contribution becomes comparable to or larger than that of the structural mass, enhancing the acoustic contrast between the two propulsion systems.

The difference in radiated sound between the two propulsion systems is primarily driven by their distinct structural acceleration levels. Since the dipole source term scales with the oscillatory force $(M + M_a)a$, even moderate variations in acceleration produce proportionally larger differences in the radiated field. The DE exhibits higher vibration amplitudes, which, when combined with the effective inertia of the surrounding fluid, result in a significantly stronger dipole contribution. Conversely, the smoother dynamic response of the HT-PEM FC leads to a weaker dipole source and therefore a lower radiated sound level, explaining the acoustic gap observed in the results.

The nature of the excitation force $F(t)$ strongly depends on the propulsion technology. In conventional DEs, the combustion process generates impulsive and periodic forces associated with pressure fluctuations and reciprocating components, which gives rise to large structural accelerations, i.e.,

$$\ddot{u}_{\mathrm{DE}} \gg \ddot{u}_{\mathrm{FC}}. \tag{14}$$

As a result, there is significant dipole radiation and, in addition, a non-negligible monopole contribution due to volumetric pulsations.

In contrast, HT-PEM methanol-based FCs operate through electrochemical processes that do not involve cyclic combustion or significant moving masses. Therefore, the excitation forces are smoother and predominantly associated with auxiliary components (e.g., pumps and compressors), leading to reduced structural vibrations and a dominant dipole contribution if compared to the monopole contribution, but with a significantly lower amplitude if compared to that of the DE.

Beyond acoustic radiation, structural dynamics may also influence the magnetic signature of the vessel. Mechanical stresses and deformations can alter the distribution of magnetization in ferromagnetic materials, introducing magnetomechanical coupling through which the mechanical stresses alter the magnetic properties of the ferromagnetic materials composing the vessel and, in turn, their magnetic response. Although this effect is secondary compared to the primary magnetic sources considered in this work, it highlights the interconnected nature of structural, magnetic, and acoustic phenomena in marine systems.

The above formulation provides a unified mechanical interpretation of acoustic radiation in marine propulsion systems. By explicitly linking material properties, structural dynamics, and fluid–structure interaction to acoustic source mechanisms, it becomes possible to rationalize the reduced noise emissions observed in fuel cell-based propulsion. From a design perspective, the minimization of the acoustic signature requires (i) a reduction in the excitation forces at the source, (ii) an increase in structural damping, and (iii) the optimization of the mass distribution to control the added mass effect. This multiphysics, mechanics-based framework therefore offers a predictive tool for the design of next-generation low-signature vessels, where the propulsion technology, structural configuration, and material selection are jointly optimized.

The structural–acoustic differences discussed above, namely the distinct acceleration levels, the resulting dipole force amplitudes, and the influence of the hydrodynamic added mass, have direct implications for both environmental impacts and underwater detectability. The reduced dipole strength of the HT-PEM FC configuration lowers the radiated pressure levels in the frequency band most relevant for marine fauna sensitivity and for passive sonar detection. Conversely, the higher low-frequency output of the diesel system increases its acoustic footprint and enhances its vulnerability to long-range detection. Thus, the mechanical and hydrodynamic differences identified in this section translate into meaningful operational and environmental consequences.

3.7. Environmental Effects on Monopole and Dipole Radiation

The analytical expressions derived in the previous sections describe the intrinsic acoustic radiation of the vessel under free-field conditions, where the surrounding fluid is assumed to be homogeneous and unbounded. In realistic marine environments, however, the received acoustic field depends not only on the source characteristics but also on the propagation conditions, which are governed by boundaries, stratification, and depth-dependent sound speed profiles.

In realistic ocean environments, reflections at the sea surface and seabed modify the spatial structure of the Green's function and, in particular, its gradient ∇G, which governs the dipole term. Because dipole radiation depends on ∇G, boundary-induced interference patterns (constructive or destructive) can enhance or suppress the dipole contribution more strongly than the monopole one, whose dependence on G is less sensitive to such gradients. Moreover, depth-dependent sound speed profiles may refract acoustic energy, producing focusing or defocusing effects that alter the relative prominence of low-frequency components. These propagation phenomena can therefore modulate the observed differences between the DE and HT-PEM FC signatures, especially in frequency bands where dipole radiation dominates. However, since both propulsion systems are evaluated under the same propagation assumptions, the comparative conclusions of this study remain meaningful: environmental effects may shift the absolute levels, but they do not alter the intrinsic difference in source strength arising from the distinct structural accelerations and monopole–dipole balances of the two propulsion technologies.

From a mathematical standpoint, all environmental effects are embedded in the acoustic Green's function. In free space, the Green's function is given by

$$G_0(\mathbf{x}, \mathbf{y}) = -\frac{e^{-ik|\mathbf{x}-\mathbf{y}|}}{4\pi|\mathbf{x}-\mathbf{y}|}, \tag{15}$$

which satisfies the Helmholtz equation in a homogeneous medium. In the presence of boundaries or inhomogeneities, the propagation is instead governed by the environmental Green's function G_{env}, defined as the solution of

$$\nabla^2 G_{\text{env}} + k^2 n^2(z)\, G_{\text{env}} = \delta(\mathbf{x}-\mathbf{y}), \tag{16}$$

where $n(z) = c/c(z)$ is the refractive index associated with depth-dependent sound speed $c(z)$.

Within this generalized framework, the acoustic pressure radiated by a compact source can be expressed as

$$p(\mathbf{x}, \omega) = M(\omega)\, G_{\text{env}}(\mathbf{x}, \mathbf{x}_s) + \mathbf{D}(\omega) \cdot \nabla G_{\text{env}}(\mathbf{x}, \mathbf{x}_s), \tag{17}$$

where $M(\omega) = i\omega\rho_0 Q$ is the monopole strength and $\mathbf{D}(\omega) = ik\mathbf{F}$ is the dipole moment. This formulation shows that environmental effects modify monopole and dipole radiation through the Green's function and its spatial gradient.

In the present study, the free-field Green's function G_0 is adopted. As a result, the computed acoustic pressure fields (Figure 3a) decay approximately as $1/r$, consistent with spherical spreading in an unbounded fluid. When expressed in terms of the SPL (Figure 3b), the curves represent the intrinsic source level (SL) and its ideal geometric spreading, without contributions from reflections or stratification.

In realistic ocean environments, the monopole and dipole components respond differently to propagation effects. The monopole term, being proportional to G_{env}, is primarily influenced by large-scale propagation paths and is only weakly sensitive to boundary-induced gradients. In contrast, the dipole term depends on ∇G_{env} and is therefore more strongly affected by reflections at the sea surface and seabed, sound speed gradients, and interference patterns. This implies that dipole-dominated sources—such as HT-PEM fuel cell propulsion systems—exhibit stronger environmental modulation of their SPLs, whereas monopole-dominated DEs are less sensitive to propagation conditions.

Although environmental effects are not included in the present calculations, the Green function formalism provides a rigorous framework for incorporating them. By separating intrinsic source characteristics from propagation, this approach enables a physically consistent comparison between propulsion technologies and clarifies how environmental conditions may alter the observed monopole and dipole contributions in operational scenarios.

4. Model Validation

In this section, to assess the physical consistency and predictive capabilities of the proposed formulation, validation against literature data is performed by comparing the results obtained according to the present acoustic model with recent measurements [16]. However, note that there are only few experimental data in the literature and, more specifically, no direct measurements of the acoustic signature of a vessel having the geometric, magnetic, and acoustic properties of the one investigated in this work.

Acoustic Signature Validation and Comparison with Experimental Data

The proposed analytical formulation of the acoustic signature is validated against established results available in the literature on URN in marine vessels. In particular, reference is made to the comprehensive framework developed within the AQUO project [16], which provides experimentally supported estimates of source levels and their decomposition into physical noise generation mechanisms. Since the experimental measurements refer to conventional vessels (diesel propulsion, propeller, and cavitation noise), while the present model also includes a fuel cell contribution, the comparison is not intended as direct source-to-source validation, but it aims to assess (1) the correctness of the spatial decay of the acoustic field and (2) the consistency of the predicted SPL within realistic ranges. According to the acoustic model, for both monopole and dipole sources, the acoustic pressure in the far-field region can be expressed in the form $p(z) \sim \frac{C}{z}$, where C is a constant depending on the source strength.

Introducing a reference position z_0, the ratio between pressures at z and z_0 is $\frac{p(z)}{p(z_0)} = \frac{z_0}{z}$. Subtracting the SPL at z_0 from that at z gives $\mathrm{SPL}(z) - \mathrm{SPL}(z_0) = 20\log_{10}\left(\frac{p(z)}{p(z_0)}\right)$, which leads to

$$\mathrm{SPL}(z) = \mathrm{SPL}(z_0) - 20\log_{10}\left(\frac{z}{z_0}\right). \tag{18}$$

This relative formulation removes the dependence on the unknown absolute source strength and allows a direct comparison between model predictions and experimental data. In this respect, it is important to note that the $1/z$ decay is strictly valid only in the far-field region. While the monopole contribution follows this behavior at all distances outside the source, the dipole field includes additional near-field terms proportional to $1/z^2$. Therefore, at short distances, the acoustic field deviates from the pure $1/z$ scaling.

In the present analysis, the comparison is performed in a range of distances where the dominant behavior is reasonably approximated by a $1/z$ dependence. As a consequence, the adopted formulation captures the main decay trend, although small deviations are expected in the near-field region.

The reference depth is chosen as $z_0 = 5$ m. This value is selected because (1) it corresponds to a region where both model predictions (Figure 2b) and experimental data are available; (2) it provides a consistent normalization point without requiring additional assumptions on the source strength. In this respect, note that this value lies in a region where near-field effects, particularly for dipole sources, are not negligible. However, the relative formulation does not assume $1/z$ behavior at $z = z_0$ but instead uses the model value at this location as a normalization point.

The subsequent variation in the SPL for $z > z_0$ is then governed by the dominant asymptotic behavior of the acoustic field. As the distance increases, the $1/z^2$ contribution becomes progressively negligible, and the field approaches the far-field regime. Therefore, the adopted formulation effectively anchors the solution in the near-field while validating the transition toward the far-field decay. No explicit adaptation of the experimental data to the geometrical characteristics of the vessel (length, beam, or draft) is performed. This is justified by the fact that the geometric spreading of the acoustic field is primarily governed by propagation physics rather than by the specific ship geometry.

Using the reference level at $z_0 = 5$ m and the relative formulation above, the comparison between the model predictions and the experimental data is shown in Figure 5. The model accurately reproduces the spatial decay of the SPL over the considered depth range, following the behavior expected from spherical spreading. The experimental data points lie consistently close to the predicted curve, indicating good agreement in both trend and magnitude. The corresponding numerical values reported in Table 3 confirm that the deviation between the model and measurements remains approximately constant and within 2 dB across all depths. This is further supported by quantitative error metrics, with a mean absolute error (MAE) and root mean square error (RMSE) both equal to approximately 2 dB and a maximum deviation of 2 dB. The comparison shown in Figure 5 and Table 3 is performed using the FC-based model curve (dipole contribution), since the DE-based prediction yields significantly higher SPL values and is not consistent with the low-noise operating conditions of the AQUO dataset.

This level of agreement supports the validity of the relative formulation adopted and demonstrates that the dominant propagation mechanism is correctly captured. Minor discrepancies can be attributed to environmental effects not explicitly included in the model, such as boundary reflections, seabed interaction, and local inhomogeneities of the water column, as well as differences in source characteristics between the modeled system and the experimental vessel. The experimental SPL values are significantly lower than those predicted for DE propulsion and are instead comparable to the FC curve. This indicates

that the experimental conditions correspond to relatively low-noise operating regimes. As a result, the acoustic signature predicted for the FC system is consistent with those of conventional vessels operating under optimized or reduced-noise conditions.

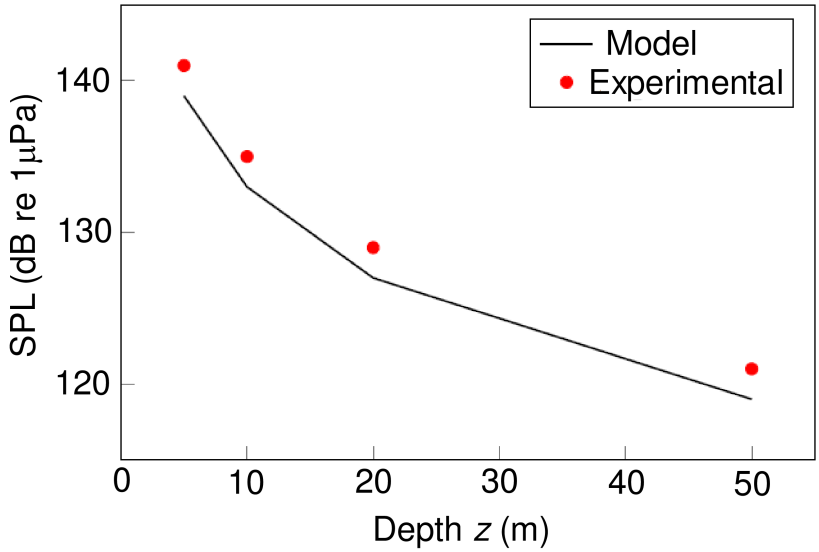


Figure 5. Comparison between model predictions (solid black line) and experimental SPL data (full red circles) as a function of depth, using $z_0 = 5$ m as a reference level.

Table 3. Comparison of SPLs as a function of depth: model (FC curve) vs. experimental data.

z (m)	SPL^{model} (dB re 1 µPa)	SPL^{exp} (dB re 1 µPa)
5	139	141
10	133	135
20	127	129
50	119	121

Overall, the comparison demonstrates that the proposed acoustic model provides a physically consistent and reliable description of the URN, particularly in terms of spatial decay and the order of magnitude.

It is important to clarify that the present validation does not aim to reproduce the absolute URN spectrum of a specific vessel, as publicly available datasets do not provide the combination of structural, geometric, and propulsion-system information required for one-to-one calibration. Instead, the validation is formulated in relative terms. The AQUO measurements used for comparison do not correspond to far-field conditions: the first data point is located at approximately 5 m from the hull, which lies within the near-field or transition-field region for a vessel of comparable size. In this range, the acoustic field is not yet governed by pure spherical spreading, and deviations from the ideal $1/r$ decay are normally expected due to the coexistence of reactive and radiative components. By contrast, the analytical model employs the free-space Green's function $G_0 = e^{ikr}/(4\pi r)$, which is strictly valid in the far field. The fact that the model still reproduces the measured pressure levels with an almost constant deviation of about 2 dB even at 5 m indicates that it captures the correct order of magnitude and spatial trend beyond its nominal asymptotic regime. This supports the use of the model for comparative purposes: the DE-FC analysis is based on relative source strengths and structural accelerations, and the adopted acceleration levels are consistent with published vibration measurements for diesel engines and low-vibration electric or electrochemical propulsion systems [35,43,44]. Consequently, the comparative

conclusions remain meaningful even if the absolute levels cannot be validated against a fully characterized reference vessel.

5. Conclusions

A comprehensive analysis of the acoustic signatures of marine vessels has been presented, with a particular emphasis on the role of fuel cell propulsion systems and their coupling with structural dynamics. The analytical monopole–dipole formulation developed in this work enables a physically transparent interpretation of the acoustic mechanisms associated with DEs and HT-PEM FCs, as summarized schematically in Figure 2. The model predicts the nearly complete suppression of the monopole term for the HT-PEM FC configuration and a reduction in the dipole pressure amplitude by approximately one order of magnitude relative to the DE, yielding SPL differences of 20–25 dB in the 20–100 Hz frequency band.

The acoustic model has been validated through comparison with experimental SPL data, demonstrating that the predicted spatial decay correctly reproduces the dominant $-20\log_{10}(z)$ trend associated with geometric spreading. The introduction of a relative SPL formulation has enabled the analysis of propagation characteristics independently of the absolute source strength, confirming the robustness of the approach when a near-field reference point is used as a normalization condition.

From a mechanical perspective, the acoustic signature is directly linked to the vibration levels of the structure and onboard machinery. The reduced acoustic emissions predicted for the HT-PEM FC system reflect its intrinsically smoother electrochemical energy conversion and the absence of combustion-driven volumetric pulsations. This leads to significantly lower structural excitation and vibration-induced noise compared with diesel propulsion, in agreement with the trends reported in recent experimental and modeling studies of fuel cell-powered marine systems.

In conclusion, the proposed methodology provides a validated and physically consistent multiphysics framework linking structural dynamics, hydrodynamic added mass effects, and acoustic radiation. The results highlight the potential of HT-PEM fuel cell propulsion for achieving substantial reductions in low-frequency underwater noise, with direct implications for the design and optimization of low-signature marine platforms. The framework developed here offers a rigorous basis for future studies aimed at integrating fuel cell technology into next-generation vessels requiring reduced detectability and enhanced vibro-acoustic performance. Finally, future work will address the influence of metamaterials and honeycomb structures on underwater noise reduction.

Author Contributions: R.Z.: Writing—Original Draft, Validation, Software, Methodology, Investigation, Formal Analysis, Conceptualization. V.C.: Writing—Review and Editing, Visualization, Supervision, Investigation, Resources, Project Administration, Funding Acquisition, Conceptualization. All authors have read and agreed to the published version of the manuscript.

Funding: This research was funded by Prog. n. RSH2A_000007-CUP: F57G25000110006.

Data Availability Statement: No research data are available.

Acknowledgments: This work has been supported by the Italian Ministry of Environment and Energetic Security in the framework of the project Piano Nazionale di Ripresa e Resilienza (PNRR)—Investimento 3.5 “Ricerca e sviluppo sull’idrogeno”, Componente 2 “Energia rinnovabile, idrogeno, rete e mobilità sostenibile”, Missione 2 “Rivoluzione verde e transizione ecologica”. (Prog. n. RSH2A_000007-CUP: F57G25000110006). R.Z. acknowledges support from Istituto Nazionale di Fisica Matematica (INdAM), Gruppo Nazionale per la Fisica Matematica (GNFM).

Conflicts of Interest: The authors declare no conflicts of interest.

Abbreviations

The following abbreviations are used in this manuscript:

a_0, b_0, c_0	Half-dimensions of rectangular prism (m)
$\mathbf{a}_p$	Hull acceleration (m s^{-2})
c	Speed of sound in water (m s^{-1})
f	Frequency (Hz)
k	Acoustic wavenumber ($k = \omega/c$, m^{-1})
p	Acoustic pressure (Pa)
p_{eff}	Effective (RMS) acoustic pressure (Pa)
p_M	Acoustic monopole pressure contribution (Pa)
p_D	Acoustic dipole pressure contribution (Pa)
p_0	Reference acoustic pressure in water (1 µPa)
r	Distance from the acoustic source (m)
$\mathbf{v}$	Acoustic particle velocity (m s^{-1})
v	Acoustic particle velocity magnitude (m s^{-1})
x, y, z	Cartesian coordinates in vessel-fixed frame (m)
α	Added-mass coefficient (–)
ω	Angular frequency (rad s^{-1})
ρ_0	Water density (kg m^{-3})
DE	Diesel engine
$\mathbf{F}_p$	Hydrodynamic force acting on the hull (N)
G_0	Free-space Green's function (m^{-1})
HT-PEM FC	High-temperature proton exchange membrane fuel cell
L_{OA}	Length overall (m)
$\mathbf{M}_s$	Structural mass matrix (kg)
M_s	Structural mass (kg)
$\mathbf{M}_a$	Hydrodynamic added mass matrix (kg)
M_a	Hydrodynamic added mass (kg)
Q	Volumetric flow rate (monopole strength) (m^3 s^{-1})
S	Control surface enclosing the source region (m^2)
SL	Source level at 1 m (dB re 1 µPa)
SPL	Sound pressure level (dB re 1 µPa)
V_{disp}	Displaced hull volume (m^3)
$\mathbf{X}$	Hull displacement amplitude (m)

Appendix A. Derivation of the Acoustic Monopole and Dipole Terms

This appendix presents the detailed derivation of the monopole and dipole acoustic radiation terms used in Section 2, starting from the Helmholtz integral formulation under linear acoustic assumptions.

Appendix A.1. Governing Equations

The acoustic pressure p satisfies the Helmholtz equation

$$\nabla^2 p + k^2 p = 0, \tag{A1}$$

with the wavenumber $k = \frac{\omega}{c}$, where ω is the angular frequency and c is the speed of sound in water. The linearized Euler and continuity equations read

$$\rho_0 \frac{\partial \mathbf{v}}{\partial t} = -\nabla p, \tag{A2}$$

$$\nabla \cdot \mathbf{v} = \frac{1}{\rho_0 c^2} \frac{\partial p}{\partial t}, \tag{A3}$$

with ρ_0 being the water density and $\mathbf{v}$ the particle velocity.

Appendix A.2. Helmholtz Integral Representation

The solution of the Helmholtz equation outside a closed surface S enclosing the source region is given by the Helmholtz integral representation

$$p(\mathbf{x}) = \int_S \left[p(\mathbf{y}) \frac{\partial G_0}{\partial n_y} - G_0 \frac{\partial p}{\partial n_y} \right] dS_y, \tag{A4}$$

where $\frac{\partial}{\partial n_y}$ is the normal derivative $\frac{\partial}{\partial n}$ at the point y with respect to the outward unit normal $\mathbf{n} = (n_x, n_y, n_z)$ to S.

Here, the free-space Green's function is

$$G_0(\mathbf{x}, \mathbf{y}) = \frac{e^{-ik|\mathbf{x}-\mathbf{y}|}}{4\pi|\mathbf{x}-\mathbf{y}|}. \tag{A5}$$

For a compact source ($|\mathbf{y}| \ll r = |\mathbf{x}|$), the Green's function can be expanded as

$$G_0 \approx \frac{e^{-ikr}}{4\pi r}(1 + ik\,\hat{\mathbf{r}} \cdot \mathbf{y}). \tag{A6}$$

Appendix A.3. Monopole Radiation Term

Retaining the leading-order term of Equation (A6) yields the p_M monopole contribution to the acoustic pressure:

$$p_M(\mathbf{x}) = -\frac{e^{-ikr}}{4\pi r} \int_S \frac{\partial p}{\partial n}\, dS. \tag{A7}$$

Applying the divergence theorem gives

$$\int_S \frac{\partial p}{\partial n}\, dS = \int_V \nabla^2 p\, dV. \tag{A8}$$

Using Equations (A1)–(A3) and mass conservation, the surface integral becomes

$$\int_S \frac{\partial p}{\partial n}\, dS = -\rho_0 \frac{d}{dt} \int_S \mathbf{v} \cdot d\mathbf{S} = -\rho_0 \frac{dQ}{dt}, \tag{A9}$$

where $Q = Q(t)$ is the volumetric flow rate through the surface S, i.e.,

$$Q = \int_S \mathbf{v} \cdot d\mathbf{S}. \tag{A10}$$

In the frequency domain, assuming harmonic time dependence $Q(t) = Q\,e^{i\omega t}$, Equation (A7) reduces to

$$p_M(\mathbf{x}) = \frac{i\omega\rho_0 Q}{4\pi r} e^{-ikr}. \tag{A11}$$

Appendix A.4. Dipole Radiation Term

The first-order term in the Green's function expansion yields the p_D dipole contribution to the acoustic pressure:

$$p_D(\mathbf{x}) = \frac{ike^{-ikr}}{4\pi r} \hat{\mathbf{r}} \cdot \int_S \mathbf{y} \frac{\partial p}{\partial n}\, dS. \tag{A12}$$

To transform the surface integral in Equation (A12), we apply the divergence theorem to the vector field $\mathbf{y}\,\nabla p$:

$$\int_S \mathbf{y} \frac{\partial p}{\partial n}\, dS = \int_V \nabla \cdot (\mathbf{y}\,\nabla p)\, dV. \tag{A13a}$$

Using the identity

$$\nabla \cdot (\mathbf{y}\, \nabla p) = \nabla(\mathbf{y} p) - p\, \mathbf{I}, \tag{A13b}$$

and noting that the term $\nabla(\mathbf{y}p)$ does not contribute to the far-field radiation of a compact source, Equation (A13a) reduces to

$$\int_S \mathbf{y} \frac{\partial p}{\partial n}\, dS = -\int_V \nabla p\, dV. \tag{A13c}$$

A second application of Gauss' theorem gives

$$-\int_V \nabla p\, dV = -\int_S p\, \mathbf{n}\, dS. \tag{A13d}$$

Using the definition of the hydrodynamic force exerted by the fluid on the hull,

$$\int_S p\, \mathbf{n}\, dS = -\mathbf{F}, \tag{A14}$$

where $\mathbf{F}$ is the hydrodynamic force exerted by the fluid on the oscillating hull.

Appendix A.5. Added Mass Contribution

For rigid-body oscillations of the hull, the hydrodynamic force can be written as

$$\mathbf{F} = -(\mathbf{M} + \mathbf{M}_a)\, \omega^2 \mathbf{X}, \tag{A15}$$

where $\mathbf{M}$ is the structural mass, $\mathbf{M}_a$ is the added-mass tensor, ω is the angular frequency, and $\mathbf{X}$ is the hull displacement amplitude.

For a hollow prismatic hull, the added mass is approximated in matrix form as

$$\mathbf{M}_a = \alpha \rho_0 V_{\text{disp}} \mathbf{I}, \tag{A16}$$

where α is the added-mass coefficient and V_{disp} is the displaced hull volume. For a prismatic shape, $\alpha \approx 1.6-2.3$. In the numerical calculations, the averaged value of $\alpha = 2$ was used. The substitution of Equation (A16) into Equation (A15) yields the final dipole pressure expression reported in Section 2.

References

1. van Biert, L.; Godjevac, M.; Visser, K.; Aravind, P.V. A review of fuel cell systems for maritime applications. *J. Power Sources* **2016**, *327*, 345. [CrossRef]
2. Zhang, Z.; Zheng, X.; Cui, D.; Yang, M.; Cheng, M.; Ji, Y. Research Progress of Fuel Cell Technology in Marine Applications: A Review. *J. Mar. Sci. Eng.* **2025**, *13*, 721. [CrossRef]
3. de-Troya, J.J.; Álvarez, C.; Fernández-Garrido, C.; Carral, L. Analysing the possibilities of using fuel cells in ships. *Int. J. Hydrogen Energy* **2016**, *41*, 2853. [CrossRef]
4. Sattler, G. Fuel cells going on-board. *J. Power Sources* **2000**, *86*, 61. [CrossRef]
5. Inal, O.B.; Deniz, C. Assessment of fuel cell types for ships based on multi-criteria decision analysis. *J. Clean. Prod.* **2020**, *265*, 121734. [CrossRef]
6. Alkaner, S.; Zhou, P. A comparative study on cycle analysis of molten carbon fuel cells and diesel engines for marine application. *J. Power Sources* **2006**, *158*, 188. [CrossRef]
7. Lucia, U. Overview on fuel cells. *Renew. Sustain. Energy Rev.* **2014**, *30*, 164. [CrossRef]
8. Briguglio, G.; Garbatov, Y.; Crupi, V. Energy and Cost Analysis of a Methanol Fuel Cell and Solar System for an Environmentally Friendly and Smart Catamaran. *Atmosphere* **2026**, *17*, 465. [CrossRef]
9. Bedi, U. Recent advances in fuel cell design and modeling: A comprehensive review. *Next Energy* **2026**, *11*, 100517. [CrossRef]
10. Gaggero, S.; Gaggero, T.; Tani, G.; Villa, D.; Rizzuto, E.; Pinto, O.; Becchi, P.; De Angelis, E.; Viviani, M. Propeller design by optimisation for underwater radiated noise reduction: A full-scale application. *Ocean Eng.* **2025**, *333*, 121412. [CrossRef]
11. Vakili, S.; White, P.; Turnock, S. Advancing a sustainable maritime future: Integrating energy efficiency and underwater radiated noise reduction strategies in commercial boating. *Mar. Pollut. Bull.* **2025**, *215*, 117835. [CrossRef]

12. Duarte, C.M.; Chapuis, L.; Collin, S.P.; Costa, D.P.; Devassy, R.P.; Eguiluz, V.M.; Erbe, C.; Gordon, T.A.; Halpern, B.S.; Harding, H.R.; et al. The soundscape of the Anthropocene ocean. *Science* **2021**, *371*, 6529. [CrossRef]
13. Erbe, C.; Marley, S.A.; Schoeman, R.P.; Smith, J.N.; Trigg, L.E.; Embling, C.B. The Effects of Ship Noise on Marine Mammals—A Review. *Front. Mar. Sci.* **2019**, *6*, 606. [CrossRef]
14. McKenna, M.F.; Ross, D.; Wiggins, S.M.; Hildebrand, J.A. Underwater radiated noise from modern commercial ships. *J. Acoust. Soc. Am.* **2012**, *131*, 92. [CrossRef]
15. Parsons, M.; Meekan, M. Acoustic Characteristics of Small Research Vessels. *J. Mar. Sci. Eng.* **2020**, *8*, 970. [CrossRef]
16. Audoly, C.; Gaggero, T.; Baudin, E.; Folegot, T.; Rizzuto, E.; Salinas Mullor, R.; André, M.; Rousset, C.; Kellett, P. Mitigation of underwater radiated noise related to shipping and its impact on marine life: A practical approach developed in the scope of AQUO Project. *IEEE J. Ocean. Eng.* **2017**, *42*, 373. [CrossRef]
17. Shipton, M.; Obradović, J.; Mišković, N.; Diamant, R. Underwater radiated noise characteristics of small vessels—An analysis of the HearMyShip database. *Mar. Pollut. Bull.* **2025**, *216*, 117903. [CrossRef] [PubMed]
18. Guo, Q.; Zhang, H.; Yang, B.; Shi, S. Underwater Radiated Noise Prediction Method of Cabin Structures under Hybrid Excitation. *Appl. Sci.* **2023**, *13*, 12667. [CrossRef]
19. Crupi, V.; Epasto, G.; Guglielmino, E.; Mozafari, H.; Najafian, S. Computed Tomography Based Reconstruction and Finite Element Modelling of Honeycomb Sandwiches under Low Velocity Impacts. *J. Sandw. Struct. Mater.* **2014**, *16*, 377. [CrossRef]
20. Scattareggia Marchese, S.; Epasto, G.; Crupi, V.; Garbatov, Y. Feasibility Study on Additive-Manufactured Honeycomb Sandwich Structural Solutions for a Fast Patrol Boat. *Compos. Struct.* **2025**, *351*, 118607. [CrossRef]
21. Armanfar, A.; Tasmektepligil, A.A.; Kilic, R.T.; Demir, S.; Cam, S.; Karafi, Y.; Abou El Majd, B.; Gunpinar, E. Embedding Lattice Structures into Ship Hulls for Structural Optimization and Additive Manufacturing. *Ocean Eng.* **2024**, *301*, 117601. [CrossRef]
22. Oliazadeh, P.; Farshidianfar, A.; Crocker, M.J. Experimental Study and Analytical Modeling of Sound Transmission through Honeycomb Sandwich Panels Using SEA Method. *Compos. Struct.* **2022**, *280*, 114927. [CrossRef]
23. Liu, Z.; Zhang, X.; Mao, Y.; Zhu, Y.Y.; Yang, Z.; Chan, C.T.; Sheng, P. Locally Resonant Sonic Materials. *Science* **2000**, *289*, 1734. [CrossRef]
24. Gao, N.; Zhang, Z.; Deng, J.; Guo, X.; Cheng, B.; Hou, H. Acoustic Metamaterials for Noise Reduction: A Review. *Adv. Mater. Technol.* **2022**, *7*, 2100698. [CrossRef]
25. Yao, D.; Zhang, J.; Lei, J.; Zhao, Z.; Zhang, Y.; Zhao, Y.; Pang, J.; Li, J. A Comprehensive Review of Acoustic Metamaterials: Applications and Challenges for Lightweight Noise Control in Large–Scale Transportation. *Mater. Des.* **2025**, *260*, 115002. [CrossRef]
26. Dong, E.; Cao, P.; Zhang, J.; Zhang, S.; Fang, N.X.; Zhang, Y. Underwater acoustic metamaterials. *Natl. Sci. Rev.* **2023**, *10*, nwac246. [CrossRef]
27. Zhu, Z.; Hu, N.; Wu, J.; Li, W.; Zhao, J.; Wang, M.; Zeng, F.; Dai, H.; Zheng, Y. A review of underwater acoustic metamaterials for underwater acoustic equipment. *Front. Phys.* **2022**, *10*, 1068833. [CrossRef]
28. Zhang, Y.; Wu, S.; Li, R.; Oh, H.; Liu, Y.; Li, J. Foldable acoustic metamaterial for underwater broadband low-frequency noise mitigation. *Phys. Rev. Appl.* **2026**, *25*, 024029. [CrossRef]
29. Qiu, Y.; Xu, W.; Hu, Z.; Fu, J.; He, M. Review of Lightweight Vibration Isolation Technologies for Marine Power Devices. *Shock Vib.* **2024**, *2024*, 1076935. [CrossRef]
30. Lu, Y.; Tang, L.; Wang, C.; Peng, Z.; Xiang, L. Low Noise Structure Design and Experimental Verification of Ship Based on Flexural Wave Band Gap Characteristics. *Materials* **2025**, *18*, 4615. [CrossRef]
31. Dong, W.; Huang, Z.; Wang, T.; Chen, M. Low-Frequency Vibration Reduction of an Underwater Metamaterial Plate Excited by a Turbulent Boundary Layer. *J. Fluids Struct.* **2024**, *126*, 104103. [CrossRef]
32. Javier, R.F.; Ramis, J.; Poveda, P.; Jesus, C.; Enrique, S. Analysis of underwater radiated noise generated by hull vibrations. *Sensors* **2023**, *23*, 1035. [CrossRef]
33. Pierce, A.D. *Acoustics: An Introduction to Its Physical Principles and Applications*; Acoustical Society of America: Melville, NY, USA, 1989.
34. Lurton, X. *An Introduction to Underwater Acoustics*, 2nd ed.; Springer: Berlin/Heidelberg, Germany, 2010.
35. Urick, R.J. *Principles of Underwater Sound*, 3rd ed.; McGraw-Hill: New York, NY, USA, 1983.
36. Dowell, E.H.; Hall, K.C. Modeling of fluid–structure interaction. *Annu. Rev. Fluid Mech.* **2001**, *33*, 445. [CrossRef]
37. Zhang, Y.; Sun, Z.; Yu, T. Vibro-acoustic coupling characteristics underwater of disc-shaped double-layer shell with stiffeners. *J. Mar. Sci. Eng.* **2025**, *13*, 1821. [CrossRef]
38. Shi, Z.; Gao, C.; Dou, Z.; Zhang, W. Flow–induced vibration modeling of bluff bodies with data assimilation. *J. Fluids Struct.* **2023**, *118*, 103844. [CrossRef]
39. Degrieck, A.; Uyttersprot, B.; Sutulo, S.; Soares, C.G.; Van Hoydonck, W.; Vantorre, M.; Lataire, E. Hydrodynamic ship-ship and ship-bank interaction: A comparative numerical study. *Ocean Eng.* **2021**, *230*, 108970. [CrossRef]
40. Holmes, J.J. *Modeling a Ship's Ferromagnetic Signatures*; Morgan & Claypool Publishers: San Rafael, CA, USA, 2007. [CrossRef]

41. Holmes, J.J. Modeling a Ship's Ferromagnetic Signatures. *Synth. Lect. Comput. Electromagn.* **2007**, *2*, 1.
42. Zivieri, R.; Crupi, V. Extended Dipole Approximation of a Ship Induced Magnetic Signature Modeled by Means of a Hollow Cylinder. *J. Magn. Magn. Mater.* **2025**, *632*, 173484. [CrossRef]
43. Hanselman, D.C. *Brushless Permanent-Magnet Motor Design*, 2nd ed.; Magna Physics Publishing: Lebanon, OH, USA, 2003.
44. Pukrushpan, J.T.; Stefanopoulou, A.G.; Peng, H. *Control of Fuel Cell Power Systems: Principles, Modeling, Analysis and Feedback Design*, 1st ed.; Springer: London, UK, 2004.
45. Ross, D. *Mechanics of Underwater Noise*; Pergamon Press: New York, NY, USA, 1976.

Disclaimer/Publisher's Note: The statements, opinions and data contained in all publications are solely those of the individual author(s) and contributor(s) and not of MDPI and/or the editor(s). MDPI and/or the editor(s) disclaim responsibility for any injury to people or property resulting from any ideas, methods, instructions or products referred to in the content.